Knee osteoarthritis automatic detection using U-Net

Ahmed Salama Abdellatif[1], Kamel Hussien Rahouma[2], Fatma E. Mansour[3]
[1]Department of Mission Control Center, Egyptian Space Agency, Cairo, Egypt
[2]Faculty of Engineering, University of Minia, Minia, Egypt
[3]Department of Physics, College of Science and Arts Methneb, Qassim University, Buraydah, Saudi Arabia

Article Info

ABSTRACT

Knee osteoarthritis or OA is one of the most common diseases that can affect the elderly and overweight people. OA is occurred as the result of wear, tear, and progressive loss of articular cartilage. Kellgren-Lawrence system is a common method of classifying the severity of osteoarthritis depends on knee joint width. According to Kellgren-Lawrence, knee OA is divided into five classes; one class represents a normal knee and the others represent four levels of knee OA. In this work, we aim to automatically detect knee OA according to the Kellgren-Lawrence classification. The proposed system uses the U-Net architecture. The overall system yielded an accuracy of 96.3% during training.

Corresponding Author:

Ahmed Salama Abdellatif
Department of Mission Control Center, Egyptian Space Agency
Cairo, Egypt
Email: ah_salama_eng_eg@yahoo.com

1. INTRODUCTION

The knee is part of a chain that comprises the lower leg, ankle, and foot below, and the pelvis, hip regions and upper leg above. All of these interact with one another and rely on one another for function and movement [1]. The knee joint is one of the most powerful and vital joints in the human body. It permits the lower leg to move in relation to the thigh while sustaining the weight of the body. The knee joint is a synovial joint that links the femur, our thigh bone and the longest bone in our body, to the tibia, our shinbone and the second longest bone in our body. The knee has two joints: the tibiofemoral joint, which connects the tibia to the femur, and the patellofemoral joint, which joins the femur and kneecap. The combination of these two joints creates a modified hinge joint, which enables the knee to straighten, bend, and rotate slightly to either side. Which joins the femur and kneecap. The combination of these two joints creates a modified hinge joint, which enables the knee to straighten, bend, and rotate slightly to either side.

Many knee problems are caused by the ageing process and the constant wear and tear on the knee joint (such as, arthritis). Other knee disorders are caused by an accident or a rapid action that stresses the knee. The following are some of the most common knee problems [2], [3]: anterior cruciate ligament injuries, arthritis, bursitis, chondromalacia, knee fracture, meniscus tears, and joint osteoarthritis (OA). OA continues to be a global public health concern, with its prevalence increasing since 1990, the researchers discovered that the global prevalence of OA increased by 113.25 percent between 1990 and 2019, 247.51 million to 527.81 million. In 1990 and 2019, the age-standardized prevalence rates (ASRs) were 6,173.38 and 6,348.25 per 100,000, respectively, with an average annual increase of 0.12 percent. ASRs of OA decreased in the hand but increased in the hip, knee, and other joints; the estimated yearly percentage changes were 0.32, 0.28, 0.18, and 0.36, respectively [4]. OA affects the knee cartilage [5], [6]. Cartilage is the tissues, which

separate the end of tibia and femur bones in knee joint. When cartilage is healthy, it allows smooth glide of bone in the joint and give enough space between knee joint bones to prevent them from rubbing each other. But in OA the cartilage top layer is breaks down and wears away, which causes the knee joint bones to rub each other causing pain.

The OA classification grades first introduced by Kellgren-Lawrence (KL) in 1957 [7], then approved by the World Health Organization (WHO) in 1961 as the definition of OA in radiology used in epidemiological research [8], [9]. KL classification depends on the join space width (JSW) measuring between the tibia and femur bones. Now days OA detection is based on clinical examination for knee joint images. There are many types of medical images which use many different technology such as magnetic resonance imaging (MRI) [10], x-ray [11], digital imaging and communications in medicine (DICOM) [12], and computed tomography (CT) [6]. Generally doctor use x-ray images to detect OA [13]. Common x-ray findings of OA include bone spur formation, joint space separation between adjacent bones, and destruction of joint cartilage. One of the major problem that face the doctor is the determine the OA grade for knee joint which require doctors with high experience to measure the distance between tibia and femur knee joint. The limitation of OA grades detection appear the need to develop a model that can automatically able to detect and classify OA. In recent years, computer vision can be used to achieve OA automatic detection. A subfield of artificial intelligence (AI) called computer vision enables gadgets to process and provide insightful data using digital images, videos, and other visual inputs. If AI allows computers to think, then computer vision allows them to see, hear, and comprehend like humans. Because of their ability to extract features, deep learning algorithms have gained a lot of traction and are being used extensively in computer vision in recent years.

The state-of-the-art deep learning technology convolution neural network (CNN) achieves the best results in image [14]. CNN is the most widely used deep learning architecture in image classification tasks, with significant performance gains since 2012 [15]. The key advantage of CNN is its capacity to autonomously extract features, such as learning separate characteristics for each class on its own. CNN is also computationally efficient since it employs pooling procedures and parameter sharing. U-Net is a special type of CNN U-Net which developed at the University of Freiburg's at Department of Computer Science for biomedical picture segmentation [16], [17]. Due the University of Freiburg's efforts in U-Net developing they gain the International Symposium on Biomedical Imaging (ISBI) 2015 Grand Challenge for computer-assisted detection of caries in bitewing radiography, as well as the cell tracking challenge in the two most difficult transmitted light microscopy categories (phase contrast and DIC microscopy) by a considerable margin. The primary distinction between CNN and U-Net, CNN change an image into a single row vector, which is commonly utilized in classification problems. However, with U-Net, an image is turned into a vector and then back to an image using the same mapping. This reduces distortion by preserving the original composition of the image. The U-Net architecture's basic structure comprises of two directions. The contraction path is the first route, also referred to as the analytical path or the encoder, and it gives categorization data like a standard convolution network. The 2nd path is an expansion path, also referred to as the synthesis path or decoder, which is made up of up-convolutions and concatenations using features from the encoder path. The network can now learn localized classification information thanks to this expansion. Furthermore, the extension path increases the output resolution, which may subsequently be passed to a final convolutional layer to create a fully segmented image. The resulting network is nearly symmetrical, with an u-shaped structure. U-Net is the most state of the art techniques that uses into segmentation.

In this work, we tend to implement an auto-segment model that automatically extracts the JSW according to KL grades using U-Net. The dataset used in this study was obtained from the National Institutes of Health (NIH), which has funded a research project at the University of California, San Francisco called the osteoarthritis initiative (OAI) to create a public domain resource to facilitate knee OA research, identify and validate knee OA biomarkers, and better understand how to prevent and treat knee OA. The ground truth images is created from the original x-ray images using visual geometry group image annotator (VIA) annotation [18]. The data augmentation is performed to increase the size of the dataset and be able to utilize the limited samples more efficiently. The proposed model accomplishes this through three main stages. The first stage is stage is determine the knee joint region; this is done based on bone density. The second stage is the image pre-processing to remove noise and enhance the image contrast; the third stage annotates the JSW by using VIA annotation programe; and the final stage creates a U-Net model to automatically extract JSW taking in consideration data augmentation to increase the number of the data set. The remainder of the paper is organized as follows; a brief summary of relevant work on knee joint segmentation is given in section 2. The techniques employed in this work will be covered in section 3. The suggested model methodology and results steps are explained in section 4. The work conclusion is presented in section 5 at last.

2. RELATED WORK

Depending on which part of the knee we want to segment, there are many different ways to perform knee segmentations. Moreover, every imaging modality has peculiarities of its own to deal with [19]. As of right now, no single segmentation technique produces results that are suitable for every type of medical image. We will quickly go over some of the most pertinent research that is connected to our methodology, e.g. knee segmentation. Gornale *et al.* [20] use a dataset consists of 2000 x-ray images which classified according KL grades with the help of two medical expert. The proposed method uses active contours algorithms to automatically knee joint after remove unwanted distortions. Then, the features is extracted from knee joint using Hu's invariant moments algorithm. The overall system is classified using The k-nearest neighbors (K-NN) algorithm classifier and decision tree classifier. K-NN classifier achive good performance than decision tree classifier, the accuracy of K-NN classifier is 99.80% and 98.65% according to medical expert 1 and 2 respectively, while decision tree classifier achieve accuracy 95.75% and 95.4% according to medical expert 1 and 2 respectively.

Wang *et al.* [21] use dataset contains of 4796 16-bit DICOM x-ray images. Their model used to automatic diagnose the OA based on deep learning. The proposed integrating the object detection model, you only look once (YOLO) with some adaptation to be suitable with knee joint structure, with the visual transformer into the diagnosis procedure. A model trained on 4.43% of annotated data can extract accurate region of interest (ROI) on the remaining data, containing more than 4500 samples. The obtained classification accuracy improves the accuracy by 2.5% compared to the traditional CNN architectures. According to Kondal *et al.* [22] the data collection contains of 4447 DICOM knee radiographs from the OAI, as well as KL grades for both the left and right knees (OAI). Images of males and females aged 45 to 79 were included in the dataset. They received the target dataset from a well-known private hospital in India, which included 1043 knee radiographs. They present a unique method for autonomously grading knee radiographs on the KL scale using a CNN. Their method is divided into two stages: in the first, an object identification model separates individual knees from the rest of the image; in the second, a regression model evaluates each knee separately on the KL scale. The proposed model was trained using the publicly accessible OAI dataset and show that fine-tuning the model before testing it on a private hospital dataset reduces the mean absolute error from 1.09 (95% CI: 1.03-1.15) to 0.28 (95% CI: 0.25-0.32). Furthermore, for the identical objective, we compare classification and regression models and show that regression outperforms classification [22].

3. MATERIALS AND METHODS

3.1. Dataset description

X-ray images were collected by NIH [23]. This dataset was organized according to KL scores. According to JSW, KL divides knee OA into five grades. The first grade (grade 0) corresponds to a normal healthy knee and the final grade (grade 4) corresponds to the most severe condition, as shown in Figure 1. The KL graduates are divided into the following categories. Grade 0: no radiographic signs of OA (cartilage loss or osteophytes). Grade 1: questionable joint space narrowing (JSN), sprouting osteophytes, bone marrow oedema (BME), and subchondral cyst. On an antero-posterior weight-bearing radiograph with BME and sub-chondral cyst, there are evident osteophytes development and a reduction in joint space width. Multiple osteophytes, de nite JSN, sclerosis, and probable bone deformation in grade 3. Large osteophytes, obvious JSN, severe sclerosis, and distinct bone deformity in grade 4. Figure 1 shows the OA grades according to KL graduates. Figure 1(a) shows OA grade 0 i.e. normal, absence of OA, Figure 1(b) shows OA grade 1 i.e. doubtful, questionable JSW with potential osteophyte formation, Figure 1(c) shows OA grade 2 i.e. mild, potential JSW with clear osteophyte formation, Figure 1(d) shows OA grade 3 i.e. moderate, clear JSW, mild osteophyte development, some disease, and ability bony end defects, and Figure 1(e) shows OA grade 4 i.e. severe, extensive osteophyte development, severe JSW with marked sclerosis, and apparent deformity of bone ends.
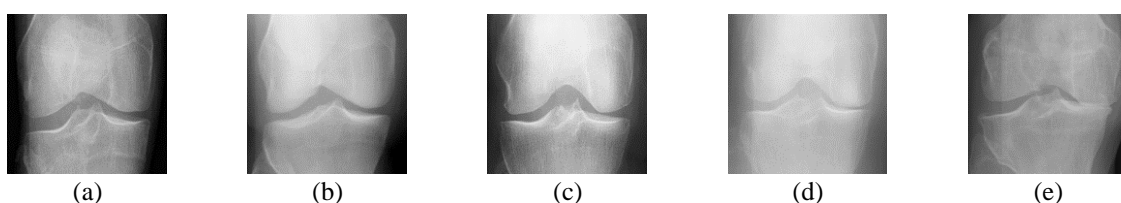

(a)	(b)	(c)	(d)	(e)

Figure 1. Knee OA severity stages (a) grade 0 (b) grade 1, (c) grade 2, (d) grade 3, and (e) grade 4

3.2. U-Net

U-Net firstly introduced in the paper, U-Net convolutional networks for biomedical image segmentation for semantic segmentation. The basic U-Net structure is similar to that of U-letter, as shown in Figure 2 [16]. The U-Net architecture mainly based on a fully convolutional network, which was first proposed by Shelhamer *et al.* [24]. The U-Net basic structure consists of a specific encoder (left path) and decoder (right path) scheme. The encoder consists of a convolution layer followed by rectified linear unit (ReLU) and path normalization to reduce the spatial dimensions. The decoder composed of a transposed convolution layer for up-sampling, after which there are two sets of convolutional and ReLU layers. The connection section consists of two sets of convolution followed by ReLU layers to join between the encoder and decoder path. The number of feature channels is doubled at each downsampling step. Every step in the expanding path starts with an upsampled feature map, which is then followed by two 3x3 convolutions, each of which is then followed by a ReLU, a 2×2 convolution ("up-convolution") that reduces the number of feature channels in half, and a combination with the correspondingly cropped feature map from the contracting path. Cropping is essential because each convolution loses boundary pixels. In order to assign each 64-component feature vector to the required number of classes, a 1×1 convolution is used at the last layer. There are twenty-three convolutional layers in the network. The operations indicated by the blue, grey, red, green, and teal arrows are respectively a convolutional operation using an 11-sized kernel and a softmax activation function that produces the final output, a copy and crop of feature maps, an up-convolutional operation using a 2×2 kernel to double the spatial resolution, and a convolutional operation using an 11×2 kernel to produce a max pooling operation. Figure 2 illustrates the U-Net structure.
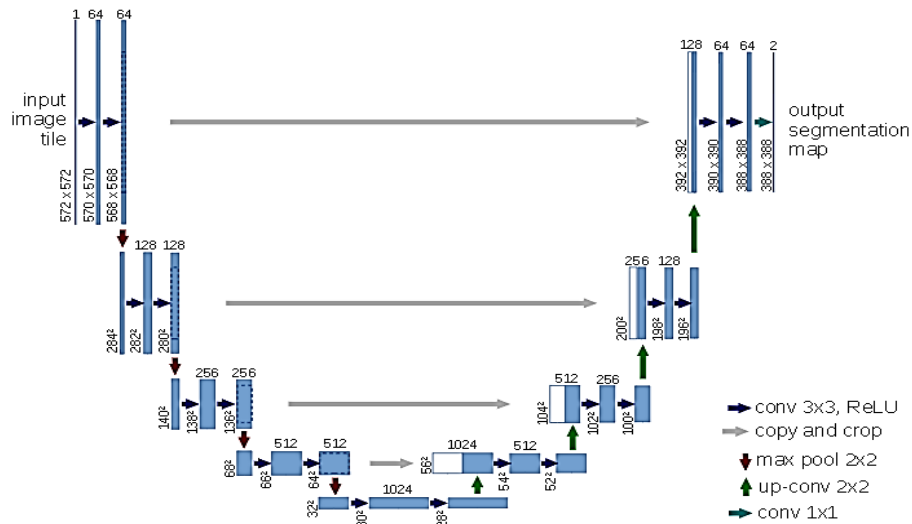

Figure 2. U-Net architecture

4.   THE PROPOSED SYSTEM ALGORITHMS

The proposed system consists of four main stages. The first stage perform localization to locate the tibia and femur intersection; the knee joint. The second stage is to perform some enhancement on the image to distinguish between the tibia, femur bones, and the knee joint. The third stage is to create the mask ground truth, which represents the knee joint. The final stage is the U-Net training model. Figure 3 shows the general suggested model structure. Figure 3(a) a sample of original image and the red rectangle represent the ROI that we aim to extract, e.g. knee joint region. Figure 3(b) the image of knee joint after extraction. Figure 3(c) perform image processing throught passing image to filters in order to enhance the image quality. Figure 3(d) create the image ground truth which created by VIA tool. Figure 3(e) shows perform training using U-Net model, the U-Net model accept two images, the original image and it's corresponding ground truth. Figure 3(f) shows after traning the model accept original knee image and produce the corresponding ROI e.g. JSW, the U-Net model tends to produce the predicated ground truth.

Stage 1: extract the knee joint region. Figure 4 illustrate this process. Figure 4(a) shows a sample of original image, which search for knee tibia and femure JSW intersection. We aim to find the red dot, starting from this point take a fix size rectangle boundary to extract the knee joint region. In order to automatically locate this point, we calculate the image row intensity and detect the lowerest point inside the red circle as

shown in Figure 4(b), calculate image column intensity and detect the lowerest point inside the red circle as shown in Figure 4(c), then find intersection between local minim intensity in rows and columns by determine the calculate tibia and femure JSW intersection which calculated as the intersection between lowset columns intensity and between lowset rows intensity as shown in Figure 4(d). Figure 4(e) create fixed size mask for knee joint according to intersection point, i.e. the calculate tibia and femure JSW intersection in previous step. Figure 4(f) shows the knee joint segment image after product the original image by created mask. One can summarize the ROI extraction according to Algorithm 1 steps.

Algorithm 1: Knee joint localization
Step 1: Read the x-ray knee image.
Step 2: Sum of gray levels of all image rows and columns.
Step 3: Determine the intersect point between low intensity for rows and columns.
Step 4: Create a fixed mask from the calculated intersection point.
Step 5: Crop the knee joint by multiply original image by the created mask.
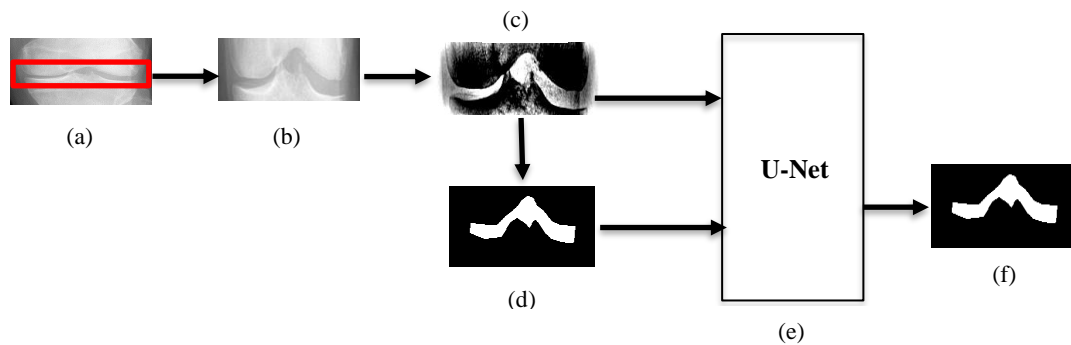
Figure 3. The suggested system's stage-by-stage order (a) original image, (b) localizationation, (c) enhancement, (d) annotation, (e) segmentation, and (e) predicated ground truth
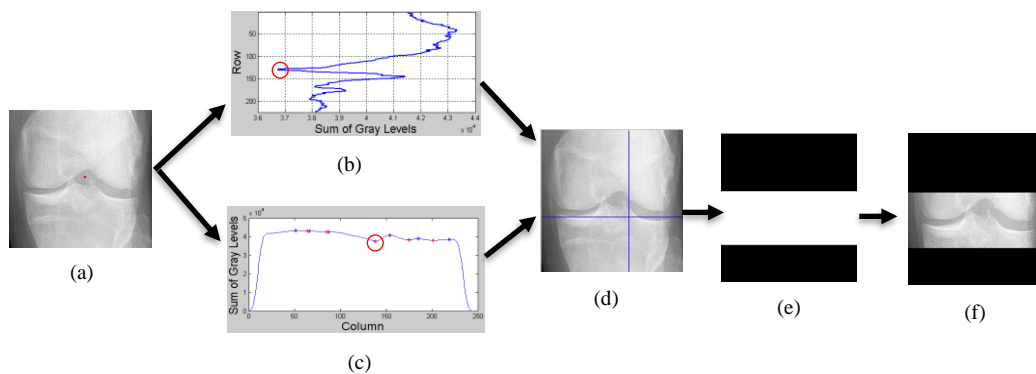

Figure 4. Knee joint localization (a) original image, (b) rows intensity sum, (c) columns intensity sum, (d) lower intensity intersectionation, (e) create maskation, and (e) crop knee joint

Stage 2: enhance the quality of image by applaying filters. Figure 5 shows the used filter. Figure 5(a) shows one original image sample that obtained from previous step. Figure 5(b) the image after applay adjust filter, i.e. maps the intensity values in grayscale image in order to increase the image contrast. Figure 5(c) shows the image after apply Gaussian filter to reducing the noise and image blurring regions. Figure 5(d) shows the image after apply average filter, i.e. smooths pixels which causes high frequency distortion. One can summarize the image enhancement procedure according to Algorithm 2 steps:

Algorithm 2: Image enhancement
Step 1: Read the x-ray knee image.
Step 2: Adjust image intensity values.
Step 3: Using a Gaussian low-pass filter with a size of 99 and a standard deviation of 16, apply the filter.
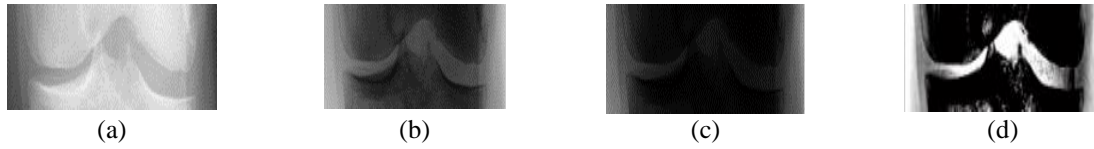Step 4: Apply average filter

Figure 5. Image enhancement (a) original image, (b) image adjust, (b) Gaussian filter, and (d) average filter

Stage 3: create ground truth. Figure 6 illustrate the annotation process. Figure 6(a) shows a sample from knee joint image that obtained from previous step. Figure 6(b) create the ground truth image using VIA tool. Figure 6(c) fill all the area inside the boundary of annotation lines, i.e. fill the gaps inside the ground truth that obtained in previous step in order to be accepted by U-Net model. The Algorithm 3 summarize the ground truth creation.

Algorithm 3: Create image ground truth mask
Step 1: Load the x-ray cropped images
Step 2: Use the via annotation tool to manually create mask for the knee joint space
Step 3: Fills holes of the annotated images

Stage 4: train the model using U-Net. In order to enhance the model accuracy, we apply augmentation to increase the data set size during training process. Figure 7 shows a sample of augmentation data. Figure 7(a) shows image sample JSW after performing enhancement, Figures 7(b)-(f) shows the correspond images generated through augmentation process to increase data set size and enhace the accuary of the training as we have limited data set. Then, the augmented data is sent as input to the U-Net for train as shown in Figure 8. Figure 8(a) shows a JSW sample image and it is corresponding grouth truth image, Figure 8(b) perform data augmentation to increase the data size, and Figure 8(c) perform training using U-Net. The Algorithm 4 list the main steps for the training using U-Net.

Algorithm 4: Create an auto-segmentation U-Net model
Step 1: Load the x-ray images with their corresponding ground truth mask.
Step 2: Augment the data to increase the number of training samples.
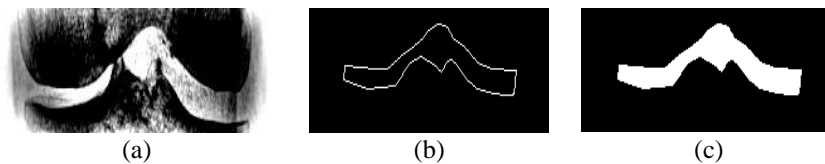Step 3: Model learning using U-Net

Figure 6. Create ground truth label (a) cropped, (b) create mask, and (c) fill holes
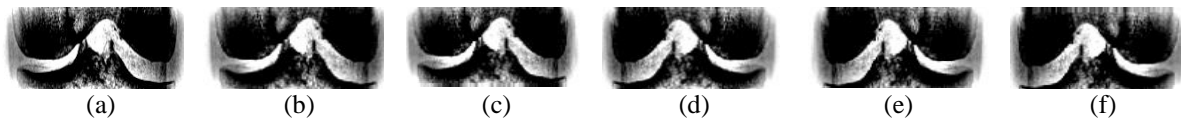

Figure 7. Sample for one image and its augmentation (a) original images, (b) augment 1, (c) augment 2, (d) augment 3, (e) augment 4, and (f) augment 5
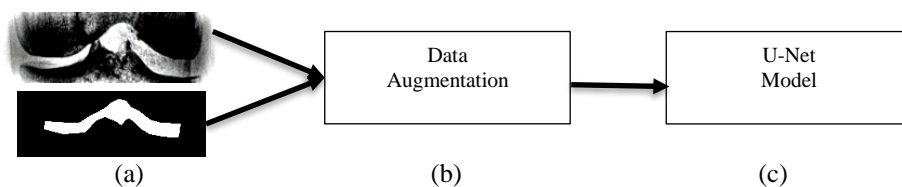

Figure 8. U-Net segmentation model (a) original image, (b) augmentation, and (c) training

5. RESULTS

In this work, we use 100 images from each OA grade; 80 images for training, and 20 images for testing. In order to evaluate the result of this work, one can use three essential metrics: intersection over union (IOU), pixel identity (PI), and localization error (LE) [25]. The system is trained for five epochs, and the batches of samples to train in each epoch are equal to 200, giving a total accuracy of 96.3%. Figure 9 shows the accuracy and loss function during the training process.

IOU is defined as the ratio between the overlapped area and the union area of the predicted segmentation image and the ground truth image. This metric takes values between zero and one; zero indicates that there is no overlap, while one indicates perfectly overlapping segmentation. The IOU score can be expressed in (1) [26]:

$$IOU = \frac{\text{true positives}}{\text{(true positives + false positives + false negatives)}} \quad (1)$$

PI accuracy is the percent of pixels in your image that are classified correctly. PI accuracy is defined by the ground truth image mask as the ratio of correctly classified pixels to all pixels in that class as declared in (2) [26]:

$$Accuracy\ score = \frac{\text{true positives}}{\text{(true positives + false negatives)}} \quad (2)$$

LE is the difference between true position and estimated position of the segmented image [27]. Table 1 shows the evacuation of the predicted masks.
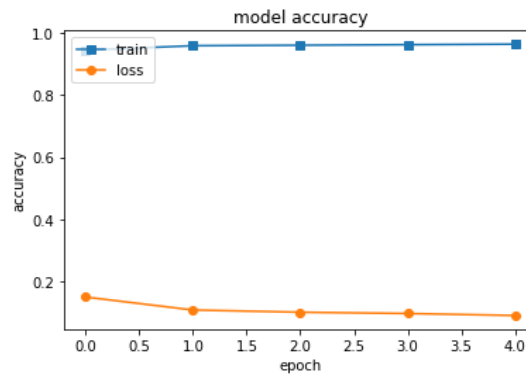

Figure 9. Model accuracy

Table 1. Predicated mask evaluation

Image No.	Grade 0			Grade1			Grade 2			Grade 3			Grade 4		
	IOU	PI	LE	IOU	PI		IOU	PI	LE	IOU	PI		IOU	PI	LE
01	0.839	0.959	11.589	0.824	0.950	3.225	0.831	0.954	1.295	0.764	0.951	2.070	0.832	0.913	12.329
02	0.847	0.953	2.471	0.806	0.947	9.598	0.840	0.957	0.895	0.769	0.949	6.963	0.704	0.931	16.662
03	0.830	0.957	4.263	0.781	0.950	26.482	0.848	0.955	3.351	0.763	0.950	3.920	0.756	0.913	11.257
04	0.832	0.955	8.384	0.788	0.947	5.950	0.801	0.954	2.928	0.791	0.951	4.410	0.896	0.940	12.368
05	0.869	0.960	0.978	0.828	0.949	0.451	0.805	0.949	3.738	0.824	0.949	5.155	0.693	0.941	7..367
06	0.839	0.954	3.305	0.799	0.950	32.057	0.847	0.955	0.889	0.799	0.952	5.060	0.781	0.833	6.368
07	0.882	0.959	0.925	0.728	0.948	0.415	0.855	0.959	0.465	0.688	0.940	43.946	0.693	0.924	63.054
08	0.861	0.952	10.247	0.831	0.950	1.481	0.857	0.955	4.133	0.739	0.937	2.313	0.615	0.922	13.629
09	0.868	0.959	3.048	0.807	0.945	4.797	0.797	0.947	7.396	0.675	0.940	2.592	0.826	0.939	10.968
10	0.869	0.957	4.743	0.825	0.953	6.158	0.813	0.940	15.397	0.776	0.952	9.052	0.759	0.941	0.589
11	0.815	0.954	3.640	0.817	0.951	6.233	0.832	0.954	1.402	0.857	0.957	0.988	0.845	0.951	4.429
12	0.852	0.958	1.528	0.848	0.958	13.121	0.834	0.959	1.308	0.758	0.946	1.176	0.827	0.928	13.598
13	0.811	0.945	16.238	0.841	0.953	6.248	0.767	0.942	1.767	0.665	0.953	31.208	0.541	0.924	77.862
14	0.822	0.956	3.899	0.808	0.945	4.748	0.801	0.943	8.110	0.762	0.941	0.575	0.650	0.926	18.960
15	0.825	0.953	7.561	0.754	0.943	4.063	0.780	0.947	10.756	0.751	0.950	6.446	0.659	0.926	12.689
16	0.838	0.951	2.590	0.709	0.936	0.086	0.788	0.948	1.435	0.741	0.945	3.812	0.892	0.880	6.358
17	0.853	0.955	5.704	0.779	0.944	8.807	0.819	0.954	14.204	0.785	0.946	4.119	0.702	0.928	38.999
18	0.848	0.954	3.679	0.779	0.944	8.807	0.868	0.958	3.720	0.753	0.948	0.650	0.775	0.949	17.488
19	0.865	0.952	5.941	0.837	0.956	1.209	0.856	0.958	1.088	0.749	0.948	2.440	0.644	0.933	31.794
20	0.831	0.955	5.700	0.819	0.952	5.537	0.878	0.955	2.108	0.803	0.956	12.497	0.891	0.948	15.367
Average	0.8448	0.9549	5.322	0.800	0.948	7.474	0.826	0.952	4.319	0.761	0.948	7.4696	0.749	0.924	20.251

6.   CONCLUSION

This study presents a model for knee for knee joint segmentation. The suggested model extracts the JSW automatically between the tibia and femur bones. The proposed model depends on the U-Net architecture. The proposed model applies to five grades of OA and achieves an average (IOU, PI, LE) of (0.8448, 0.9549, 5.322), (0.8, 0.948, 7.474), (0.826, 0.952, 4.319), (0.748, 0.924, 20.251) for grade 0 to grade 4.

REFERENCES

[1]   A. W. J. M. Glaudemans, R. A. J. O. Dierckx, J. L. M. A. Gielen, and J. H. Zwerver, *Nuclear medicine and radiologic imaging in sports injuries*. Berlin, Heidelberg: Springer, 2015, doi: 10.1007/978-3-662-46491-5.
[2]   L. F. Samhan, A. H. Alfarra, and S. S. Abu-Naser, "An expert system for knee problems diagnosis," *International Journal of Academic Information Systems Research (IJAISR)*, vol. 5, no. 4, pp. 59–66, 2021.
[3]   S. Kwon, W. Kim, S. Yang, and K. H. Choi, "Influence of the type of occupation on osteoarthritis of the knee in men: The Korean National Health and Nutrition Examination Survey 2010-2012," *Journal of Occupational Health*, vol. 61, no. 1, pp. 54–62, 2019, doi: 10.1002/1348-9585.12022.
[4]   J. Wan, X. Qian, Z. He, Z. Zhu, P. Cheng, and A. Chen, "Epidemiological trends of hand osteoarthritis from 1990 to 2019: Estimates from the 2019 Global Burden of Disease study," *Frontiers in Medicine*, vol. 9, 2022, doi: 10.3389/fmed.2022.922321.
[5]   S. M. Ahmed and R. J. Mstafa, "A comprehensive survey on bone segmentation techniques in knee osteoarthritis research: from conventional methods to deep learning," *Diagnostics*, vol. 12, no. 3, pp. 1-26, 2022, doi: 10.3390/diagnostics12030611.
[6]   H. Villarraga-Gómez, E. L. Herazo, and S. T. Smith, "X-ray computed tomography: from medical imaging to dimensional metrology," *Precision Engineering,* vol. 60, pp. 544–569, 2019, doi: 10.1016/j.precisioneng.2019.06.007.
[7]   J. H. Kellgren and J. S. Lawrence, "Radiological assessment of osteo-arthrosis.," *Annals of the rheumatic diseases*, vol. 16, no. 4, pp. 494–502, 1957, doi: 10.1136/ard.16.4.494.
[8]   E. M. Macri, J. Runhaar, E. H. G. Oei, and S. M. A. Bierma-Zeinstra, "Kellgren/Lawrence Grading in Cohort Studies: Methodological Update and Implications Illustrated Using Data From a Dutch Hip and Knee Cohort," *Arthritis Care & Research*, vol. 74, no. 7, pp. 1179–1187, 2022, doi: 10.1002/acr.24563.
[9]   J. Mischlinger *et al.*, "Long-term persistence of antibodies after diphtheria/tetanus vaccination in immunosuppressed patients with inflammatory rheumatic diseases and healthy controls," *Vaccine*, vol. 40, no. 33, pp. 4897–4904, 2022, doi: 10.1016/j.vaccine.2022.06.013.
[10]   S. Geethanath and J. T. Vaughan, "Accessible magnetic resonance imaging: A review," *Journal of Magnetic Resonance Imaging*, vol. 49, no. 7, pp. e65–e77, 2019, doi: 10.1002/jmri.26638.
[11]   P. J. Withers *et al.*, "X-ray computed tomography," *Nature Reviews Methods Primers*, vol. 1, no. 1, pp. 1-21, 2021, doi: 10.1038/s43586-021-00015-4.
[12]   D. A. Clunie, "DICOM format and protocol standardization—a core requirement for digital pathology success," *Toxicologic Pathology*, vol. 49, no. 4, pp. 738–749, 2021, doi: 10.1177/0192623320965893.
[13]   B. Darlow *et al.*, "Living with osteoarthritis is a balancing act: An exploration of patients' beliefs about knee pain," *BMC rheumatology*, vol. 2, no. 1, pp. 1–9, 2018, doi: 10.1186/s41927-018-0023-x.
[14]   C. F. G. D. Santos and J. P. Papa, "Avoiding overfitting: a survey on regularization methods for convolutional neural networks," *ACM Computing Surveys (CSUR)*, vol. 54, no. 10, pp. 1–25, 2022, doi: 10.1145/3510413.
[15]   K. Rahouma and A. Salama, "Knee images classification using transfer learning," *Procedia Computer Science*, vol. 194, pp. 9–21, 2021, doi: 10.1016/j.procs.2021.10.055.
[16]   W. Weng and X. Zhu, "INet: Convolutional networks for biomedical image segmentation," *IEEE Access*, vol. 9, 2021, pp. 16591–16603, doi: 10.1109/ACCESS.2021.3053408.
[17]   H. Xu, X. Chen, P. Qian, and F. Li, "A two-stage segmentation of sublingual veins based on compact fully convolutional networks for Traditional Chinese Medicine images," *Health Information Science and Systems*, vol. 11, no. 1, 2023, doi: 10.1007/s13755-023-00214-1.
[18]   A. Dutta and A. Zisserman, "The VIA annotation software for images, audio and video," in *MM 2019 - Proceedings of the 27th ACM International Conference on Multimedia*, 2019, pp. 2276–2279, doi: 10.1145/3343031.3350535.
[19]   G. F. Baker, G. J. Tortora, and N. P. A. Nostakos, *Principles of Anatomy and Physiology*, New York, USA: John Wiley & Sons, 1976, vol. 76, no. 3, doi: 10.2307/3423898.
[20]   S. S. Gornale, P. U. Patravali, and P. S. Hiremath, "Automatic detection and classification of knee osteoarthritis using hu's invariant moments," *Frontiers in Robotics and AI*, vol. 7, pp. 1-8, 2020, doi: 10.3389/frobt.2020.591827.
[21]   Y. Wang, X. Wang, T. Gao, L. Du, and W. Liu, "An Automatic knee osteoarthritis diagnosis method based on deep learning: data from the osteoarthritis initiative," *Journal of Healthcare Engineering*, vol. 2021, 2021, pp. 1-10, doi: 10.1155/2021/5586529.
[22]   S. Kondal, V. Kulkarni, A. Gaikwad, A. Kharat, and A. Pant, "Automatic Grading of Knee Osteoarthritis on the Kellgren-Lawrence Scale from Radiographs Using Convolutional Neural Networks," in *Advances in Deep Learning, Artificial Intelligence and Robotics*, Cham: Springer, 2022, pp. 163–173, doi: 10.1007/978-3-030-85365-5_16.
[23]   I. Štajduhar, M. Mamula, D. Miletić, and G. Ünal, "Semi-automated detection of anterior cruciate ligament injury from MRI," *Computer Methods and Programs in Biomedicine*, vol. 140, pp. 151–164, 2017, doi: 10.1016/j.cmpb.2016.12.006.
[24]   E. Shelhamer, J. Long, and T. Darrell, "Fully convolutional networks for semantic segmentation," *IEEE transactions on pattern analysis and machine intelligence*, vol. 39, no. 4, pp. 640-651, 2017, doi: 10.1109/TPAMI.2016.2572683.
[25]   D. Müller, D. Hartmann, P. Meyer, F. Auer, I. Soto-Rey, and F. Kramer, "MISeval: A metric library for medical image segmentation evaluation," *Studies in Health Technology and Informatics*, vol. 294, pp. 33–37, 2022, doi: 10.3233/SHTI220391.
[26]   "Evaluate semantic segmentation data set against ground truth," *MathWorks*, 2017. Access date: Oct. 07, 2023. [Online]. Available:. https://in.mathworks.com/help/vision/ref/evaluatesemanticsegmentation.html.
[27]   P. Sermanet, D. Eigen, X. Zhang, M. Mathieu, R. Fergus, and Y. LeCun, "OverFeat: Integrated Recognition, Localization and Detection using Convolutional Networks," *2nd International Conference on Learning Representations, ICLR 2014-Conference Track Proceedings*, pp. 1-16, 2014.

BIOGRAPHIES OF AUTHORS
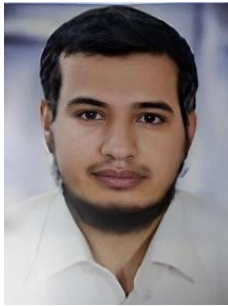
Ahmed Salama Abdel Latif earned his B.Sc. in Communications and Electronic Engineering from the Faculty of Engineering, Cairo University in 2003. He earned his Diploma in Computer Science from Institute of Statistical Studies and Research, Cairo University in 2014. He earned his M.Sc. in Electrical Engineering from the Faculty of Engineering, Al-Azhar University in 2016. He earned his Ph.D. in Electrical Engineering from the Faculty of Engineering, Minia University in 2023. Now he has worked as a software analysis team leader at the Egyptian Space Agency. He is experienced in satellite ground stations, data analysis, parallel programming, and artificial intelligence systems. He can be contacted at email: ah_salama_eng_eg@yahoo.com.

Kamel Hussein Rahouma earned his B.Sc. and M.Sc. in Communications and Electronic Engineering from the Faculty of Engineering, Cairo University in June 1984 and March 1988 respectively. He earned his first doctoral degree in Communications and Electronics Engineering jointly from the University of Kent at Canterbury (England) and Minia University (Egypt) in 1996. In May 2001, he earned his second doctoral degree in Computer Science from the University of Salzburg, Austria. Currently he is a vice dean of the Faculty of Computer Science, Nahda University, Beni Suef, Egypt. He can be contacted at email: kamel_rahouma@yahoo.com.

Fatma Elzahraa Mansour earned her master degree in biophysics from Mansoura University in 2008. She earned her doctoral degree in biophysics from Mansoura University in 2014. Currently she is associated professor in the College of Science and Arts, Qassim University, Saudi Arabia. She can be contacted at email: f.mansur@qu.edu.sa.